# Effect of Swirl Ratio on Charge Convection, Temperature Stratification, and Combustion in Gasoline Compression Ignition Engine

**Ashutosh Jena, Harsimran Singh, Avinash Kumar Agarwal***

Engine Research Laboratory, Department of Mechanical Engineering,

Indian Institute of Technology Kanpur, Kanpur-208016, India

Corresponding author's email: akag@iitk.ac.in

## Research Highlights

- The impact of in-cylinder flows on GCI combustion.
- Effect of swirl on flow structures and impact on charge transport.
- The formation of lean mixture zones was identified.
- Potential zones of HC formation were explored.
- In-cylinder flows and charge transport used for piston modifications.

**Contributions by authors**:

**Ashutosh Jena**: Conceptualisation, software, validation, analysis.

**Harsimran Singh**: Literature review, analysis, editing, draft writing.

**Avinash Agarwal**: Supervision, facility acquisition, review of results, Final editing.

# Effect of Swirl Ratio on Charge Convection, Temperature Stratification, and Combustion in Gasoline Compression Ignition Engine

**Ashutosh Jena, Harsimran Singh, Avinash Kumar Agarwal***

Engine Research Laboratory, Department of Mechanical Engineering,

Indian Institute of Technology Kanpur, Kanpur-208016, India

Corresponding author's email: akag@iitk.ac.in

## Abstract

Various low-temperature combustion (LTC) strategies [namely homogeneous charge compression ignition (HCCI), reactivity controlled compression ignition (RCCI), partially premised charge compression ignition (PCCI)] have shown the potential to comply with upcoming and prevailing stringent emissions legislations. Low octane gasoline has emerged as an ideal fuel candidate for premixed charge combustion under diesel-like conditions in gasoline compression ignition (GCI) engines. GCI is an excellent technology to rectify future global energy demand imbalance because it aims to replace diesel (which is in short supply) with low octane fractions (LOF)/ naphtha (which is in surplus supply) in CI engines. However, this novel combustion concept requires modifications in the conventional design of diesel engines. The combustion chamber shape and in-cylinder flows play a crucial role in charge distribution and temperature stratification. Therefore, understanding the combined effect of combustion chamber geometry and in-cylinder flows is essential for future engine designs. GCI combustion engine simulations for varying swirl ratios (SR) were performed in CONVERGE CFD software to understand the effect of in-cylinder air motion on the mixture stratification and combustion. A 1/7$^{th}$ sector geometry for a conventional re-entry piston bowl was modeled and then simulated. Two different mechanisms were used for model validation. The results indicated that the large-scale flow structures govern the fuel distribution in the combustion chamber. The charge convection because of increased swirl has a substantial effect on the combustion characteristics of the engine. A distinguished ignition kernel was observed for all test cases. An interfacial region with counter-rotating vortices formed a lean mixture zone, hindering flame propagation and combustion. A lower SR, shallow depth piston, and modifications to avoid flame quenching in the squish zone need to be further investigated to optimize the engine performance.

**Keywords:** Gasoline compression ignition; Low-temperature combustion; Mixture stratification; Swirl.

# I. Introduction

Low production cost, proven robustness, and compactness continue to make the internal combustion (IC) engines attractive prime movers for vehicles and other industrial machines in the twenty-first century, 140 years after their first demonstration. Spark ignition (SI) and compression ignition (CI) engines have their pros and cons. Inspite of that, direct injection compression ignition (DICI) engines have emerged as a powerplant of popular choice for small-to-large vehicles because of their higher energy conversion efficiency.[1] The major challenge for DICI combustion is the well-known NOx-PM trade-off. The formation of lean fuel-air mixtures in the vicinity of high-temperature flames and locally fuel-rich reaction zones ($\Phi_{local} > 2$) is the primary reason for NOx and PM formation, respectively, in the combustion chamber.[2-3] One way to control the NOx and PM emissions simultaneously is by installing advanced exhaust gas after-treatment devices. For instance, selective catalytic reduction (SCR) has been used widely to reduce NOx emissions. In contrast, diesel particulate filters (DPF) are the most effective devices to limit PM emissions. Research has been carried out to integrate SCR and DPF functions by wash-coating the SCR catalyst on the DPF substrates.[4-7] No doubt, this will lead to the development of compact and improved thermal management of the after-treatment systems; however, it will also add to the cost of the vehicles. The other option involves the reduction of pollutant formation during combustion. It requires that combustion occurs at comparatively lower peak in-cylinder temperatures (1500-1800K) to limit NOx formation. The heat release must be delayed until adequate air-fuel mixing has taken place to limit PM formation.[8] Researchers also proposed a set of low-temperature combustion (LTC) technologies, used widely to address the NOx-PM trade-off without affecting the thermal efficiency. Although advanced diesel combustion technologies can efficiently reduce harmful emissions, premixed charge preparation before the combustion remains a challenge.[9] Gasoline compression ignition (GCI) is a promising LTC technology that takes advantage of higher volatility and auto-ignition temperature of gasoline-like fuels/ low octane fractions (LOF) and higher compression ratios of diesel engines.[8-12] LOF's with research octane numbers (RON) between 50-80, known as naphtha, are relatively lesser processed streams than diesel and gasoline in a refinery.[13] A low octane number and hence longer ignition delay helps form a more homogenous charge in the engine, which controls NOx and soot formation simultaneously. Out of other mixing-related design variables, swirl and piston bowl geometry have been used widely to control the soot by aiding the preparation of a homogeneous charge. Increasing the dwell between the 'end of injection' (EoI) and the 'start of combustion' (SoC) is a crucial aspect of these designs. Jena *et al.*[14] concluded that piston pip shape and gradient substantially affect the piston bowl vortices and turbulent kinetic energy (TKE) of the flow, affecting mixture stratification and combustion. Therefore, piston bowl geometry and swirl ratio (SR) must be examined together to achieve optimum engine performance benefits. Bowl-in-piston designs are commonly used in CI engines to promote fuel-air mixing because they increase the in-cylinder turbulence. However, gasoline is quite different from diesel in both the chemical composition and the physical properties. Gasoline-like fuels showed a longer flame lift-off length compared to diesel. Also, the liquid penetration length of diesel spray was 1.8-2.4 times longer than gasoline.[11] Because of significant differences in diesel and gasoline-like "fuels' chemical composition and physical properties, their spray-bowl interactions are bound to be quite different. Therefore, it becomes essential to optimize piston bowl geometry and apply initial boundary conditions specifically for gasoline-like fuels; however, it would be quite challenging to investigate this experimentally. Lab-based steady flow models have been used to understand the flow dynamics and gas exchange processes for variable geometries. This approach facilitates experimenting with a large number of prototypes but may lead to sub-optimal results.[15] Compared to experiments, engine simulation provides flexibility to change design parameters in a broader range in lesser time and cost while maintaining acceptable accuracy. Several studies have focused on turbulence and flame kernel growth interactions through direct numerical simulations (DNS). However, most of these studies adopted simplified reaction mechanisms and simplified geometries due to higher computational costs.[16-17] Therefore, most engine simulations and optimization studies were done either using the Unsteady Reynolds Average Navier Stokes (URANS) equation approach or the Large Eddy Simulation (LES) approach. Because of its powerful diagnostics capabilities, dedicated 3D simulation software 'CONVERGE-CFD' has been widely used by various researchers for predicting in-cylinder combustion processes, flow dynamics, mixture formation, spray characteristics, and combustion acoustics. Many experimental and numerical research studies discussed various factors affecting CI combustion as well. Kodavasal *et al.*[18] performed closed-cycle CONVERGE CFD simulations of a GCI engine. They reported that for retarded combustion with an increasing SR, standard explanation, i.e., reduced equivalence ratio and over-lean mixture packets because of high SR, were no longer valid since the Φ-T diagrams were almost similar for both SR cases. They concluded that lower SRs must be preferred because they maintain higher in-cylinder temperatures, aiding in auto-ignition in the GCI engine. Dolak *et al.*[19] used multi-objective optimization algorithms (NSGA-II) and CFD solver to optimize light-duty diesel engines. They concluded that stepped piston bowls with lesser SRs exhibited minimum soot particle numbers in cases when the outer and inner bowls were 80% and 60% of the bore diameter. Fridriksson *et al.*[20] studied the effect of four different piston geometries on heat transfer. Compared to the stepped piston bowl, tapered piston bowl geometry consistently showed higher thermal efficiency and NOx emissions due to higher peak combustion temperatures. However, the reduction in the heat loss in the conventional diesel piston bowl was higher than the chamfered re-entrant and tapered lip-less piston at lower SRs. Pastor *et al.*[21] performed an optical study to examine the effect of three-piston geometries (re-entrant bowl and hybrid bowl consisting of stepped lip and wave geometry) on the combustion in a light-duty CI engine. High-speed combustion images revealed that the wave protrusions enhanced the soot oxidation by avoiding the flame to flame interactions on the piston bowl periphery and redirected flames towards the piston bowl center. Cao *et al.*[22] analyzed the effect of three different piston geometries on the PCCI combustion and emissions. They reported that the fuel near the upper edge of the re-entrant bowl evaporated relatively later than the vertical side piston bowl and the open piston bowl. This was due to the formation of low-temperature regions because of the evaporative cooling effect. Also, earlier ignition was observed in the case of the open piston bowl. Several researchers explored the effect of swirling flows to optimize combustion and emissions. Kook *et al.*[23] reported a reduction in ignition delay and advancement of the early heat release with an increasing swirl. Benajes *et al.*[24] concluded that increased SR did not increase the mixing process in late-cycle combustion. Higher swirl numbers could worsen the combustion event by unreasonable spray overlapping, resulting in a slower heat release and lower indicated thermal efficiency.

As discussed above, many studies explored the effect of swirl motion and piston bowl geometry on the CI combustion fueled with mineral diesel. The significant differences in GCI combustion were due to differences in physical properties of gasoline, such as the boiling point and chemical properties compared to diesel, which in turn affected the in-cylinder mixing and combustion processes. Therefore, the development of a specifically tuned combustion chamber design is essential to extract optimum GCI engine performance. Researchers are therefore exploring innovative piston geometries for GCI engine emission compliance. However, the impact of flow dynamics from the design standpoint has not been explored yet. The piston geometry and swirl dictate the large-scale turbulence structure in the combustion chamber. Besides, for fuels with longer ignition delay, the convection time scales are smaller than the delay period; therefore, the charge convection and temperature stratification play a pivotal role in the piston design. In this study, the impact of variations in SRs on combustion is investigated. Hence the main objective of this study is to develop a deeper understanding of the role of large-scale structures on the charge distribution and in-cylinder mixing processes in a GCI engine combustion chamber.

## II. Computational Fluid Dynamics Model Description

The commercial CFD software CONVERGE 3.0 was used to perform closed cycle simulations. Since the injector has seven equispaced nozzle holes, 1/7$^{th}$ of the combustion chamber was modeled using a sector simulation approach to conserve computational time and cost. Engine specifications are provided in Table 1. Figure 1 shows the modeled combustion chamber with grid refinement from the fixed embedding and the adaptive mesh refinement (AMR). The in-cylinder turbulence was simulated using the Renormalization group (RNG) $k$-$\varepsilon$ model. The blob injection model developed by Reitz and Diwakar[25] was used to simulate the atomization of liquid fuel spray/ droplets. This model is based on continuous injection of fuel droplets in the gas phase, having a size equal to the effective orifice diameter of the nozzle.

The subsequent breakup of the injected liquid blob and droplets were modeled employing Kelvin-Helmholtz (KH) and Rayleigh-Taylor (RT) mechanisms. This model incorporated the effect of the Kelvin-Helmholtz waves driven under the influence of aerodynamic forces with Rayleigh-Taylor instabilities induced by retardation of shed drops in the free stream. In this model, droplet breakup was decided by the minimum breakup time predicted by either KH or RT model.[26] SAGE model[27] was used to account for the detailed chemistry and combustion. Generally, a minimum grid size of 0.25 mm is suggested for the diesel combustion simulation. In this case, the base grid size was set at 0.7 mm. AMR of level 2 (for both temperature and velocity) was used, resulting in a mesh size of 0.175 mm to resolve the velocity and temperature gradients accurately. Fixed embedding was used to resolve the near nozzle flow field using two different reaction mechanisms. Mechanism 1 was obtained by merging the two different skeletal reaction mechanisms, viz. iso-octane and heptane.[28,29] These skeletal mechanisms were based on semi-decoupling methodology. The mechanism for flame propagation depends largely on the kinetics of small radicals and molecules, and hence it was decoupled from the low-temperature chemistry. However, smaller molecular fragments and low-temperature chemistry were used in the coupling, affecting fuel's ignition characteristics. Mechanism 2 was adopted from Liu *et al.*[30], which was a reduced PRF mechanism. This was based on the addition of the skeletal chemical kinetic model of toluene (56 species and 168 reactions) to their previously developed PRF mechanism[28] consisting of 48 species and 152 reactions considering 87% iso-octane and 13% n-heptane (by mass) as fuel surrogate. This mechanism was extensively validated with experimental results of different reactors. Table 2 shows the initial and boundary condition used for the simulation.

Table 1. Engine Specifications

| | |
|---|---|
| Bore × stroke (mm) | 82 × 90.4 |
| Displacement ($cm^3$) | 477.2 |
| Compression ratio | 17.8 |
| Connecting rod length (mm) | 145.4 |
| Number of nozzles | 7 |
| Nozzle hole diameter (mm) | 0.141 |
| Injector umbrella angle (deg) | 148 |
| Swirl ratio | 2.2 |

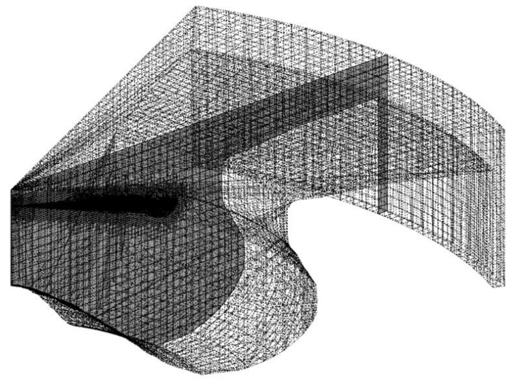

Figure 1. 1/7th sector mesh at -17°aTDC showing embedding around spray plume and AMR

Table 2. Initial and boundary conditions

| | |
|---|---|
| Injected mass (mg/cycle) | 9.68 |
| Engine Speed | 1500 |
| $P_{IVC}$ (bar) | 1.38 |
| $T_{IVC}$ (K) | 391 |
| $T_{liner}$ (K) | 380 |
| $T_{head}$ (K) | 400 |
| $T_{piston}$ (K) | 400 |
| Starting of simulation (°aTDC) | -132 |
| End of simulation (°aTDC) | 60 |
| Kinetic Mechanism | Liu *et al.*[30] |
| Iso-octane (% by mass) | 87 |
| n-heptane (% by mass) | 13 |

## III. CFD Model Validation

The in-cylinder pressure curve was compared with the experimental pressure curve[31] to validate the model at -24°aTDC injection timing with the engine running at 1500 rpm. Injection timing was set as SoI of -21° aTDC to account for the injection lag of 3° CA, as obtained from the experiments. Thus SoI of -21° aTDC will be used in the subsequent sections. Crevices were added to the sector mesh, and CR was modified for superior validation of results without changing the squish height. Disturbing the squish height is generally not recommended because squish height significantly affects the late-cycle compression flow dynamics, affecting the combustion kinetics adversely. The experimental and predicted pressure curves are shown in Figure 2.

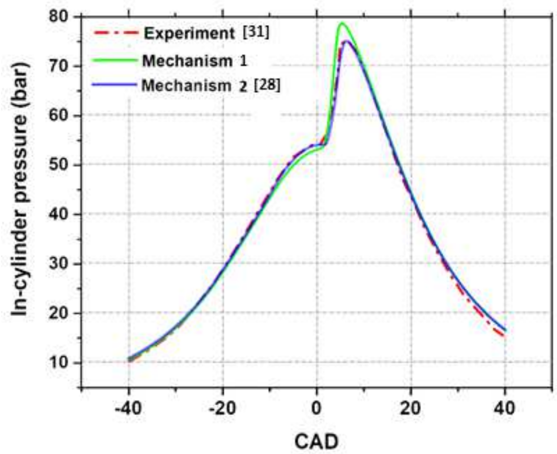


Figure 2. Comparison of in-cylinder pressure predictions by simulations using two mechanisms vis-à-vis experimental results[31]

Mechanism 1 was also able to predict the SoC; however, the RoPR was slightly higher than the experiment. Therefore the model predicted higher peak pressure. The mechanism proposed by Liu *et al.*[30] matched the pressure curve with a maximum error of 4.2%, which is acceptable. The peak pressures and pressure rise rates were also predicted with negligible error. After this validation, Mechanism 2 (Liu *et al.*[30]) was used for further investigations.

# IV. Results and Discussion

### A. Effect of Swirl Ratio on Combustion

Figure 3 shows the in-cylinder pressure variations with the crank angle degree for different SRs. As the SR increased from the baseline (SR 2.2), the SoC got delayed. A similar trend was also reported in previous studies.[18] This is counter-intuitive because increased mixing was expected to advance the combustion in higher swirl cases.

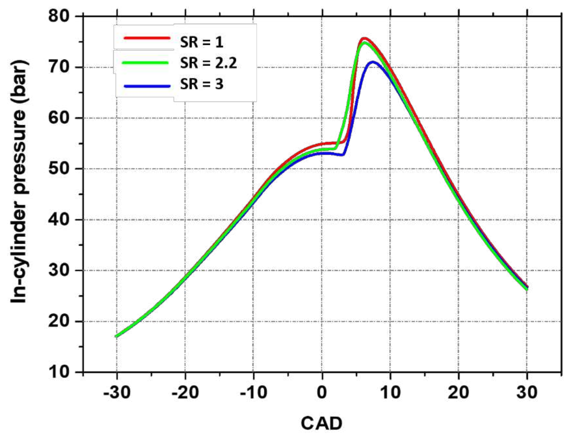


Figure 3. Pressure vs. CAD curves for the three SRs

For the high swirl case, the spray plume experienced more deflection in the downstream direction of the swirl motion than the low swirl case after traveling a sufficient distance downstream of the nozzle hole. This leads to significant vapor distribution and formation of over-lean air-fuel mixture packets, which results in delayed 'end of combustion' (EoC) (longer combustion duration) up to a point where the piston has moved sufficiently downwards in the power stroke. Thus, a major part of combustion occurs in a comparatively larger in-cylinder space, leading to a lower peak in-cylinder pressure than SR = 2.2. The SR 1 case resulted in retarded SoC. Higher RoPR and peak pressure were observed in this case.

Figure 4 depicts the apparent heat release (AHR) calculated using the first law of thermodynamics and the in-cylinder pressure data. Higher AHR was observed for the lowest swirl case. For SR 2.2 and SR 3, the AHR eventually merged. However, a higher fraction of the heat was released later in the cycle for SR 3 case.

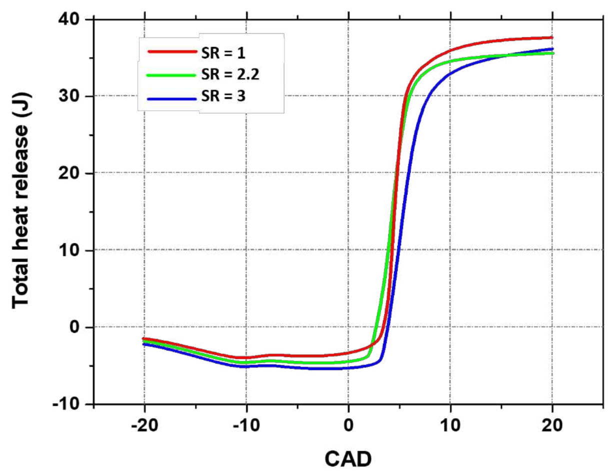


Figure 4. Apparent heat release vs. CAD for all three SRs

Figure 5 shows the SoC, combustion phasing (CP), and EoC for all SRs under investigation. SoC ($CA_{10}$) is the crank angle position corresponding to 10% cumulative heat release (CHR), CP ($CA_{50}$) is the crank angle position corresponding to 50% CHR, and the EoC ($CA_{90}$) is the crank position corresponding to 90% CHR.

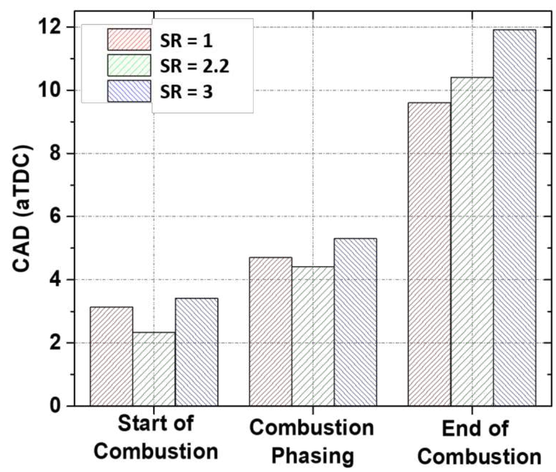


Figure 5. Combustion parameters for SR =1.0, 2.2, 3.0

As noted in Figure 5, the SoC gets retarded by decreasing or increasing the SR from 2.2. A similar trend was observed for the CP as well. The combustion for SR 1 accelerated in the last phase. SR 1 exhibited $CA_{90}$ before SR 2.2. Detailed analysis of the in-cylinder processes is required for a complete understanding of these observations.

**B. Spray-Swirl Interactions and Turbulence**

Stratification of temperature and charge governs the SoC, and the initial heat release rate (HRR) and turbulence play a pivotal role. The mixing of fuel and air is directly affected by the in-cylinder turbulence. The wall heat transfer coefficient depends on near-wall turbulence, which affects the temperature distribution in the combustion chamber.

Turbulent flows are characterized by Reynolds fluctuating equations. By simplifying and averaging, the material transport of TKE (k) is obtained as:

$$\frac{Dk}{Dt} = P + D - \varepsilon \tag{1}$$

Where P stands for turbulence production, D is the transport term, and ε is the viscous dissipation term. The turbulence production, P, is given by

$$P = -\overline{u_i' u_j'} \frac{\partial \bar{u}_i}{\partial x_j} = -\langle u_i' u_j' \rangle \langle S_{ij} \rangle \tag{2}$$

where, $u_i'$ *and* $u_j'$ are the fluctuating velocities, and <$S_{ij}$> is the strain tensor, which stands for the deformation rate of the fluid parcel. In diesel engines, the late compression flows are significantly affected by the swirl-squish interaction. The mean rate of strain tensor in the swirl squish plane (r-$\theta$) can be expressed as:

$$\langle S_{r\theta} \rangle = \frac{1}{2}\left(\frac{1}{r}\frac{\partial \langle U_r \rangle}{\partial \theta} + \frac{\partial \langle U_\theta \rangle}{\partial r} - \frac{\langle U_\theta \rangle}{r}\right) \tag{3}$$

Where, $U_r$ and $U_\theta$ represent the velocities in radial and azimuthal directions, respectively. Under motoring conditions, the axial symmetry is assumed; therefore, the first term $\left(\frac{1}{r}\frac{\partial \langle U_r \rangle}{\partial \theta}\right)$ representing the gradient of radial velocity in azimuthal direction vanishes. However, the spray swirl interaction would create a gradient in tangential velocity in the azimuthal direction, which would be affected by the momentum transfer from the spray and the intensity of the swirl.

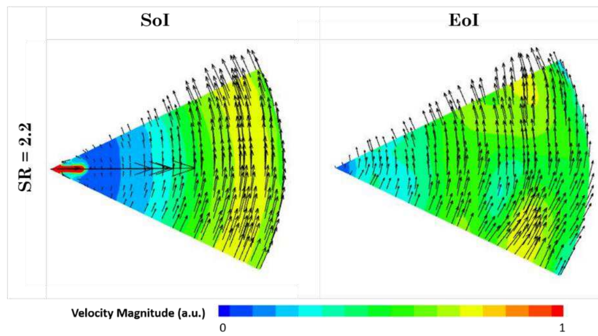


Figure 6. Velocity magnitude contours at start of injection (SoI) and end of injection (EoI)

Spray also transports the low-velocity fluid from the piston-bowl center to the outer regions. Figure 6 shows the velocity magnitude distribution in the spray plane for SoI and EoI. The velocity distribution was symmetric before the spray penetrated. However, the low-velocity fluid was transported with the spray, and the gradient was evident at the EoI. Therefore, the spray interaction with the different swirl conditions is important in turbulence generation and charge distribution.

### C. Global TKE Variations with Swirl

Figure 7 shows the variations of global TKE as a function of CAD for the simulated SRs. The injection timing (- 21° aTDC) was kept constant for all cases.

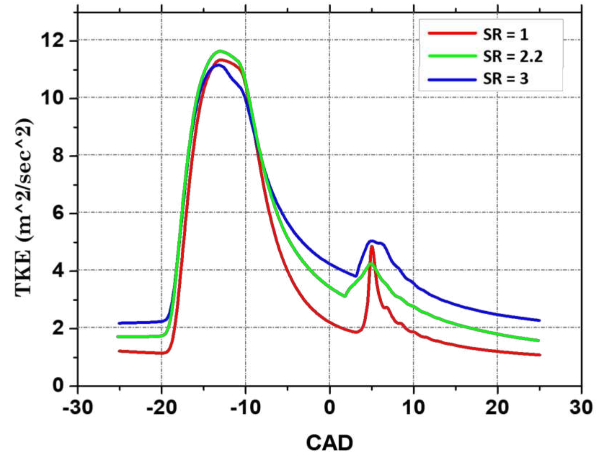


Figure 7. Global TKE variations as a function of crank angle

The simulations predicted relatively higher in-cylinder TKE for higher SR before the start of injection (SoI). Higher angular momentum of the in-cylinder fluid for higher SR resulted in a steeper gradient in the velocity hence higher turbulent stresses. The TKE increased rapidly with the injection event for all three cases. The impulse of the injected spray jet formed vortices due to a high-velocity gradient between the ambient and the jet. Thermal gradient due to higher evaporation of gasoline-like fuels under high-temperature conditions may also affect the turbulence generation. This contributed to an increased turbulence intensity in the cylinder. Experimental studies have reported that the turbulence levels can increase up to 4 times depending on the injection timing due to spray-swirl interactions.[32] Also, turbulence generated near TDC is more likely to be amplified. The TKE values attain a peak after the mid injection and then decay rapidly as the injection concludes. The SR 2.2 case achieved the maxima TKE during injection, while the SR 3 case decayed at a relatively slower rate. TKE of SR 3 was the maximum before the SoC amongst the three investigated SRs. The second peak in the curve is a result of combustion-induced turbulence.

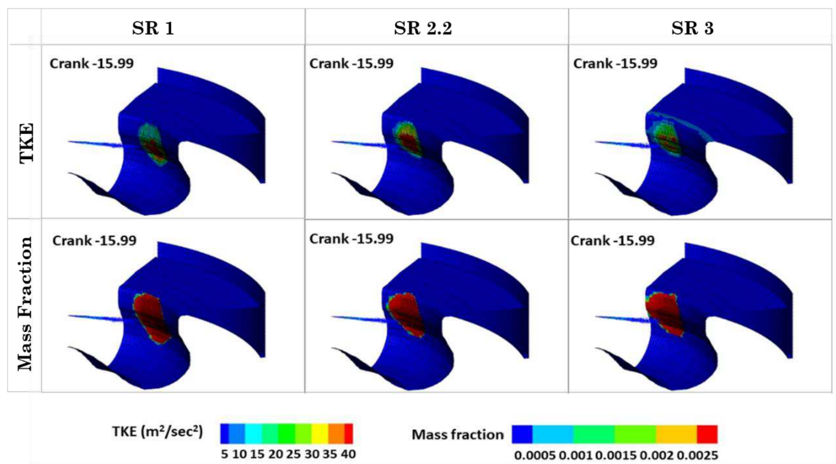


Figure 8. TKE and fuel mass fraction distribution in the vicinity of spray impingement location

A higher rate of TKE increase was observed for lower SRs. This could be attributed to a sharp rise in HRR and the maximum in-cylinder pressure ($P_{max}$). Overall, the maximum global TKE due to spray-swirl interactions was largely unaffected by the SR. However, a higher rate of decay was observed for a lower SR. To further analyze the behavior of global TKE, an analysis of spray-induced turbulence and spray wall impingement was done. The momentum distribution by high-pressure jets plays a crucial role in turbulence generation. The angular momentum of the swirl resulted in higher mass and momentum accumulated towards the outer region of the piston bowl; therefore, the near nozzle velocity field remained relatively weaker.[33] The magnitude and frequency of the near nozzle flow play a vital role in exciting the instabilities on the spray jet. The nature of excitation becomes insignificant in the far-field of the jet. Hence, for large bore engines, the near nozzle field may not be quite crucial. However, the turbulent jets are confined in the combustion chamber for small-bore engines, similar to the one used in this study. Characteristic differences in near nozzle flows may significantly affect the downstream fuel-air mixing in the combustion chamber.[34] The results depicted that the spray injection velocity was at least an order of magnitude higher than the near nozzle velocity field. Thus, the early stage of spray evolution and penetration is not affected significantly by the in-cylinder flow dynamics. On the other hand, the droplet velocity and droplet diameter distribution downstream of the injector are significantly affected by the flow field in the ambient. Sharma et al.[35] compared the spray evaluations under quiescent and engine-relevant conditions and reported significant differences in the flow velocities in both cases. The flow velocity downstream of the spray jet is determined by the level of swirl and spray-swirl interactions in the combustion chamber. In another study, the laws applicable between the flow field conditions and the maximum stable diameter of the droplets were demonstrated using experiments and numerical methods.[36] Figure 8 shows the variations of in-cylinder TKE (first row) and mass fraction (second row) at -15.99° aTDC for SR 1.0, 2.2, and 3.0. Figure 8 showed that the liquid penetration of the fuel spray plume was almost similar for all three cases. However, liquid spray-wall impingement of gasoline was not predicted in any of these test cases. Typically, in the case of high-pressure diesel injection, a significant amount of spray-wall impingement takes place.

The liquid spray has very high momentum; hence the near-wall turbulence is also very high. A higher mass fraction of iso-octane (low boiling point fraction) in the test fuel results in early evaporation; therefore, the steady-state penetration of the liquid spray does not reach the wall. Figure 8 (First row) shows the TKE near the spray impingement location for the three SRs investigated. At –16° aTDC, the spray reached the steady-state, though the injection continued till -10° aTDC. The turbulence near the spray target region was affected by the downward moving squish flow and the momentum carried by the impinging vapor cloud. The SR 2.2 case exhibited the maximum near-wall TKE, followed by SR 1 and SR 3. As discussed earlier, the evaporation of fuel droplets started much earlier upstream of the wall.

Thus, the evaporated mass convected along with the swirl decreased the momentum transfer in the radial direction. This was more pronounced in higher SR cases. The mass fraction of the impinging jet also confirmed this observation. The swirl direction was anti-clockwise when viewed from the top. Figure 8 (bottom row) clearly showed that for the SR 3 case, the impingement was biased in the direction of the swirl. The momentum of the impinging spray can be related to the fuel injection pressure (FIP), which increases the injection velocity, hence the momentum. It was observed that higher FIP resulted in earlier wall impingement and turbulent convection.[37] Therefore, for the SR 1 case, more fuel vapors impinged along the spray axis. This resulted in higher intensity gas vortex near the wall, further increasing the turbulence. Due to earlier spray impingement, their energy also dissipated quickly due to wall shear, as evident from figure 7, which showed global TKE variations. This also explains the lower peak for the SR 3 case. The radially convected vapor mass impinges later along the stream, resulting in delayed momentum transfer to the near-wall region. TKE for SR 3 case decayed at a  slower rate than lower SR cases.

### D. Effect on Wall Heat Transfer and Temperature Stratification

Wall heat transfer plays a key role in temperature distribution before the auto-ignition. Temperature stratification determines the onset of auto-ignition and HRR in the premixed combustion. Heat loss during combustion leads to a reduction in thermal efficiency. Figure 9 below shows the distribution of convective heat transfer coefficient (CHTC) right before the auto-ignition (first row) and right after the SoC (second row) for all SRs investigated.

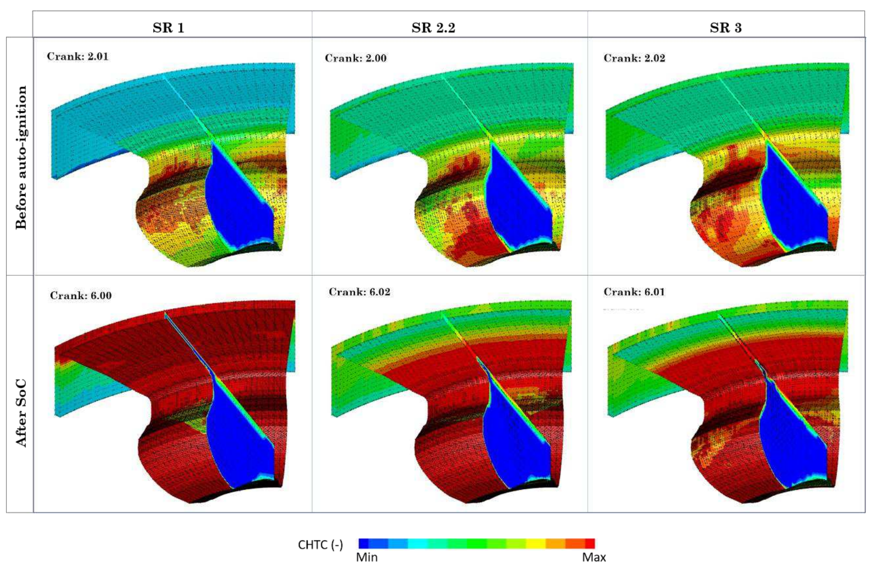


Figure 9. Convective heat transfer coefficient (CHTC) variations just before the auto-ignition (first row) and just after the SoC (second row) for all SRs

Before the SoC, the piston bowl region exhibited a higher CHTC compared to squish and crevice regions. The turbulence created by the impinging spray and the vertical plane vortices formed in the piston bowl due to the squish-swirl interactions were the primary reasons for this observation. At the piston bowl periphery, CHTC values were almost similar for all test cases. As discussed in the previous section, the impinging spray momentum was higher for the lower SR case (SR 1), leading to a more significant contribution by the spray-induced turbulence near the wall. This was similar to an impinging jet with higher FIP. Perini *et al.*[38] also predicted higher wall heat transfer at higher FIPs due to a higher impinging jet velocity. The tangential velocity of the in-cylinder swirl increased along the radius from the center to the periphery. Therefore, the near-wall velocity was higher for the higher SRs. For SR 3 case, CHTC was the maximum near the cylinder wall (inside the crevice) among the three cases investigated. However, a lower value of CHTC was observed in the squish region. The distributions shown were in the expansion stroke near the TDC (2° aTDC) when the piston was nearly stationary. At this point, the squish velocity was negligible; the head and piston boundary effects slowed down the tangential velocity in this region, which resulted in relatively lower CHTC. This observation was identical for all three cases and more pronounced for the higher SR case.

After the combustion started, a sudden rise in temperature and pressure occurred in the piston bowl. The expanding gases pushed the bulk of the remaining charge into the squish region. This was evident from the downward motion of the piston and anti-squish flow during the expansion stroke. High velocity expanding gases produced a significant turbulent shear in the squish zone; hence CHTC increased rapidly. One interesting observation was that increase in heat transfer was the maximum for the lowest SR case. This was attributed to a sharp rise in RoPR and HRR for the lowest SR case (SR 1). Higher RoPR increased the gas velocity in the region. This was also evident from the global TKE curve, where the sharp rise of TKE after combustion was observed for the lowest SR case (SR 1).

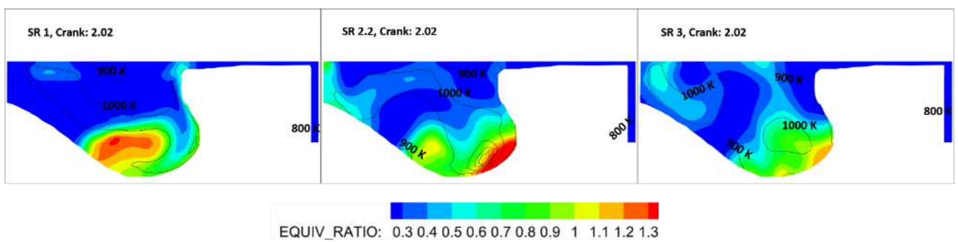


Figure 10. Distribution of equivalence ratio just before the SoC

Figure 10 depicts the charge distribution along with temperature stratification in the piston bowl. The plane shown in the figure was 10° CA downstream of the spray along the direction of the in-cylinder swirl, which was anti-clockwise when viewed from the top. The equivalence ratio contours represent the charge distribution, while the temperature gradient is shown by lines enclosing regions of the same temperature. The figure shows that superior fuel distribution was achieved by the highest SR case (SR 3). In contrast, most of the fuel accumulated near the periphery for the lower SR case (SR 1). The role of large-scale vortices is evident here. Counter-rotating vortices present in the SR 3 case split the spray vapor into two regions: the central and outer zones. A strong gradient in the velocity was created at the common interfacial region of these two vortices, which deformed the mean flow in the swirling plane, resulting in small-scale turbulent structures. These structures led to over-mixing in this region.[23] Therefore, a lean mixture zone was formed between the central piston bowl and the peripheral region. A similar distribution was observed for the SR 2.2 case. However, a relatively richer mixture zone was formed near the piston bowl center. As the SR increased, the vortex location also changed, and the interface between the rotating vortex shifted closer to the periphery.[14] Therefore, superior distribution of fuel occurred for the SR 3 case compared to SR 2.2 case. The convection of charge in the swirl direction is also important. This was higher for the SR 3 case, which enhanced the mixing in the swirling plane. The fuel distribution observed for the SR 1 case was quite different from the other two cases investigated. The bulk of the charge remained near the periphery, and an insignificant charge accumulation was predicted in the piston bowl. In previous sections, this was highlighted that a higher momentum gets convected in the radial direction for the lowest swirl case. As the SR decreased, a single dominant structure filled the entire piston bowl region.[23] Hence, in this case, the charge distribution was dominated by the re-entrant geometry of the piston bowl. After the onset of spray wall impingement, the fuel vapors followed the piston bowl geometry path along with the flow structure. Fuel accumulation near the piston lip and squish zone was observed for the SR 1 case. Relatively leaner distribution was found for the SR 2.2 case, while no charge accumulation was seen in SR 3 case in the same region. This was attributed to higher impinging spray momentum for the lowest swirl case, which decreased with swirl due to charge convection in the swirling plane.

The temperature stratification predicted was significantly different among all three cases. For SR 1 case, the maximum temperature was seen below the piston lip region. The region with the highest equivalence ratio exhibited a lower temperature. The high-temperature pocket was from the center of the piston bowl to the periphery and concentrated along the spray plume path, away from the boundary. For SR 2.2 case, the maximum temperature occurred near the re-entry point in the piston bowl. For the SR 3 case, discrete pockets of high-temperature zones were observed near the central region and the peripheral region, separated by the interfacial region of vortices, as discussed earlier. Thus, the higher turbulence and mixing near the interfacial region also affected the temperature stratification. A closer review revealed that the temperature stratification was governed by the location and nature of vortices formed. For SR 1, a single vortex dominated, which minimized the fuel-air mixing; hence, the stratified pocket was parallel to the spray axis. The charge distribution seems to be affected by the wall temperature only. For the SR 2.2 and SR 3 cases, the pockets were disturbed by the strong re-entrant flow vortices near the interface. The effect was more pronounced for SR 3 case, splitting the pocket into two due to over-mixing.

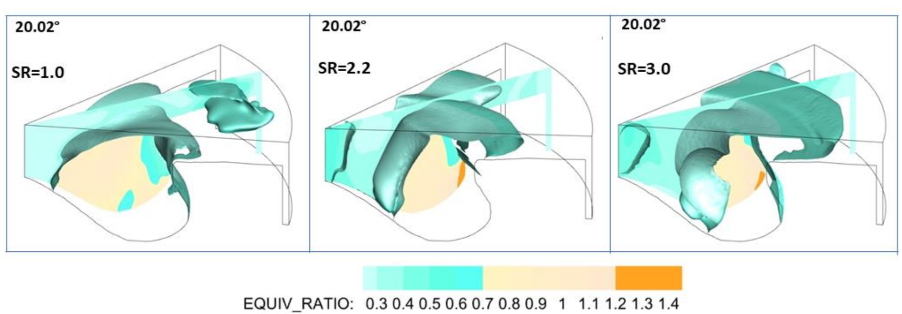

Figure 11. The iso-thermal surfaces at 1200K and Φ variations

Figure 11 shows the temperature iso-surfaces after $CA_{90}$ for all three cases. A temperature iso-surface was generated for T = 1200 K. The concave region formed by the iso-surface and the domain boundary represents T > 1200 K. Above 1200K temperature, the probability of oxidation of UHC increases significantly. This oxidation of UHC is further promoted in the zones having an intermediate stoichiometric range between 0.7 to 1.2. The equivalence ratio, as well as the temperature, determine the mixture reactivity. From figure 11, it can be observed that favorable conditions for UHC oxidation occur in the piston bowl at the outer regions. For SR 1, the iso-surface is seen near the cylinder boundary in the squish region. Furthermore, the iso-surface covered a higher charge volume in the piston bowl than the other two cases investigated. For higher swirl ratios, low temperature and lean mixture zones were observed near the cylinder wall. However, higher piston-bowl center temperature was observed for SR 2.2 and SR 3. A relatively leaner and lower temperature zone was formed near the piston-bowl center for the SR 1 case. From this, it can be concluded that the near injector region at a lower swirl ratio could be a potential source of UHC, whereas the interfacial region and squish region formed low reactivity mixtures for a higher swirl ratio leading to unfavorable conditions for UHC oxidation. Further analysis has been provided in the subsequent section with formaldehyde (HCHO) as a marker of UHC emissions.

**E. Low Temperature and High-Temperature Heat Release**

Formaldehyde is perceived as an indicator of low-temperature heat release (LTHR), while OH radical intensity indicates high-temperature heat release (HTHR) in the LTC.[39] In the LTHR phase, the fuel molecules undergo a chain branching reaction, resulting in free radicals. These free radicals assist in auto-ignition, and the main heat release occurs in the HTHR phase. Figure 12 shows the distribution of formaldehyde mass fraction at three different crank angles for each SR investigated. The crank angles close to the SoC, CP, and EoC were chosen.

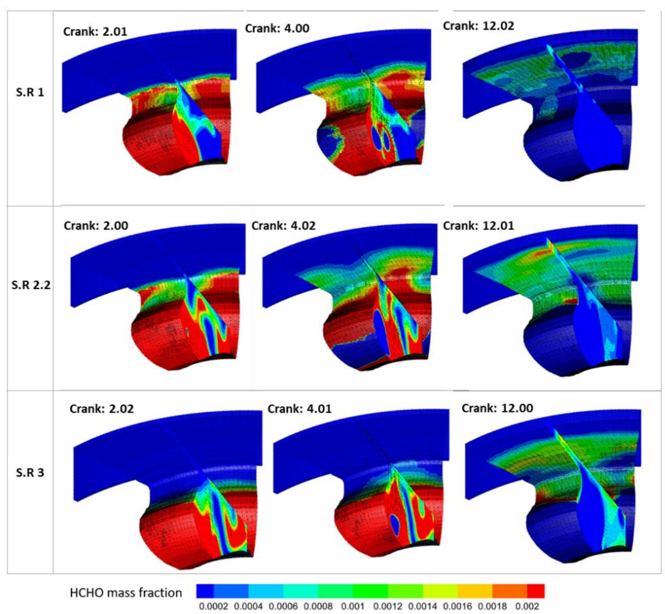


Figure 12. Formaldehyde (HCHO) distribution as a marker of LTHR

Formaldehyde formation started near the EoI for all three cases. The distribution of formaldehyde was similar to the equivalence ratio distribution, i.e., rich mixture zones were also the zones of higher formaldehyde concentrations. An experimental study by Tang *et al.*[40] reported similar observations. For SR 1 case, most of the formaldehyde was concentrated near the piston bowl periphery. The central piston bowl region was completely free of formaldehyde traces. The formaldehyde distribution for SR 2.2 and SR 3 was almost similar. However, overmixing near the interfacial location of the vortices was more pronounced for SR 3 case. The simulation also predicted no fuel penetration into the squish region before the SoC for all three cases. When the HTHR begins, formaldehyde gets consumed quickly.

Two distinct ignition kernels were observed for SR 1 case, which merged later on. These kernels were formed in the richer mixture zones, slightly centrally inside the piston bowl. For the other two cases, the ignition kernel was closer to the piston bowl periphery. It could be noted from the equivalence ratio and temperature distribution contours that the combustion started near the region of $\Phi \sim 1.2$, and a temperature of ~1000 K. Gas expansion in the combustion region pushed the remaining charge into the squish zone. For SR 1 case, the bulk of the charge was close to the periphery, which underwent rapid combustion. This was also evident from the higher peak pressure of the same case. For SR 2.2 and SR 3 cases, the flame could not propagate through the lean mixture zone formed due to over-mixing. Therefore, traces of formaldehyde were observed near the central piston bowl region for these two higher swirl cases after the EoC. This contributed to higher HC emissions from the engine. A recent study by Raman et al.[41] also concluded that the central piston bowl region might be a major source of HC emissions in partially premixed combustion (PPC) engines. Vortex-flame interactions also play a crucial role in premixed charge combustion. Increased turbulence intensity due to vortex stretching may result in flame extinction, leading to higher UHC emissions.[42] Interestingly, for SR 1 case, no formaldehyde traces were left in the central bowl region. However, the richer pockets formed resulted in a sharp increase in the rate of pressure rise (RoPR). Therefore, a shallow piston bowl with less steep re-entry could lower HC emissions while keeping the RoPR low due to superior mixture homogeneity. However, this needs further numerical and experimental investigations.

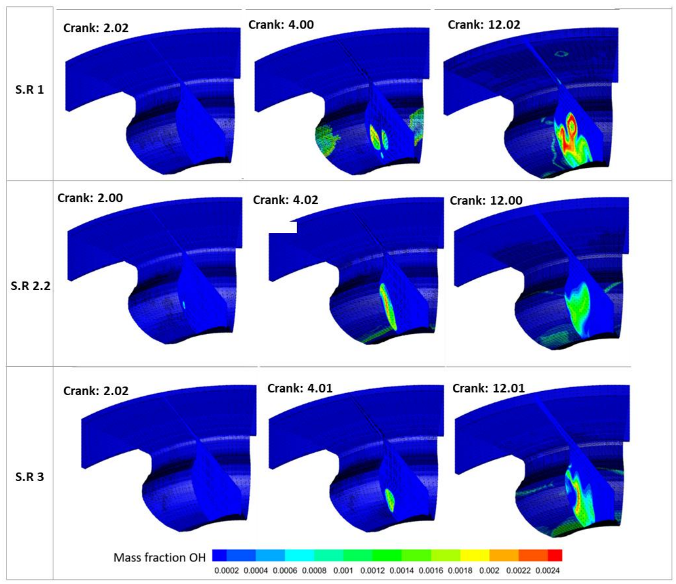


Figure 13. In-cylinder OH radical mass distribution at $CA_{10}$ (first column), $CA_{50}$ (second column), $CA_{90}$ (third column) for all swirl cases

The development of the ignition kernel can also be seen from the OH radical mass concentration shown in figure 13. The OH radicals first appeared in locations where formaldehyde disappeared. As the formaldehyde formed during the LTHR is consumed, this marks the onset of HTHR. The OH radicals last up to the EoC in the piston bowl. For the SR 1 case, a higher OH radical concentration was observed, which covered a greater area than the other two cases. OH radicals attack and oxidize soot particles. A longer residence time of the OH radicals in the piston bowl, especially in a fuel-rich zone, helps reduce soot emission.[43] Higher charge containments inside the piston bowl promote complete combustion with less fuel entering the squish region. Hence superior combustion efficiency was achieved for SR 1 case. This was also evident from figure 4, where higher AHR was observed for SR 1 case.

## V. General Discussion

It is important to appreciate the difference between conventional diesel combustion (CDC) and premixed gasoline combustion. In diesel engines, liquid spray impingement is inevitable in small bore engines. The extent of liquid **fuel** impingement affect**s** the temperature stratification near the wall. The temperature gradient may affect the vorticity of the counter-rotating vortices and hence the wall heat transfer.[44] However, the simulations predicted the absence of liquid fuel impingement on the walls due to the lower boiling point of the fuel and higher charge convection during the fuel injection process. In CDC, the re-entry of the spray droplets is governed by the momentum of impinging fuel droplets and combustion chamber shape. The interfacial region of the two vortices directs the unburned fuel from the periphery and fresh oxygen from the center to common regions. However, due to increased vaporization, a significant amount of fuel may also get trapped near the central piston bowl region in the GCI engine. This delayed combustion also provides sufficient time for charge convection and mixing, which results in the formation of lean boundary, as observed in the higher swirl case. The premixed combustion governs combustion acoustic signature. Therefore, the GCI combustion is expected to be noisier than the CDC and diesel LTC.[45] In diesel LTC, formaldehyde is formed near the spray jet's vortex head, covering the entire spray jet. This is different from the present observation. In GCI combustion, formaldehyde appears much earlier during the fuel injection process and around the periphery of the spray jet. Significantly higher premixing time leads to the distribution of formaldehyde in the piston bowl. Unlike diesel LTC, the OH radical concentration covered a higher area and penetrated the piston bowl center for the lower SR case. Because of a longer dwell time between the EoI and the SoC, GCI combustion might approach HCCI combustion. However, unlike HCCI, clear and distinct ignition kernels were observed during the GCI combustion. A strong gradient confirmed the charge stratification in the piston bowl. This was experimentally verified in a study as well.[40] The combustion started inside the piston bowl near the edge. However, this may change depending on the SoI, which directs the bulk of the fuel into the squish region and the crevices, particularly in advanced injection timings.[41]

## VI. Conclusions

The objective of this study was to simulate the mixture formation and charge convection in a conventional diesel engine using low octane gasoline as the test fuel. The SR was varied to simulate different flow dynamics in the combustion chamber. Two different reaction mechanisms were used and experimentally validated. The impact of flow structures on temperature stratification, heat transfer, and combustion is explored and discussed. Liquid spray impingement was not evident; however, the vapor convection was significantly affected by the swirl. No fuel penetration into the squish region occurred before the auto-ignition in the piston bowl for all three cases, wherein the ignition kernels developed in the piston bowl edge. Expanding gases pushed the charge into the squish zone. Incomplete combustion was evident in this region due to higher heat losses, resulting in lower temperatures, leading to flame quenching. This phenomenon was more pronounced in higher SR cases. A single vortex structure dominated the lower SR case, which promoted superior charge distribution and flame transport towards complete combustion. For higher SR cases, two counter-rotating vortices were observed. The interfacial region of these vortices formed a lean mixture zone, forbidding the flame propagation towards the center of the piston bowl. Therefore, piston design must incorporate vertical plane vortices and their role in charge convection. Further investigations at varying engine loads and speeds should be undertaken for optimizing the GCI engine design for emission compliance.

## References

[1] Singh, A. P., & Agarwal, A. K. (2018). Utilization of alternative fuels in advanced combustion technologies. In *Prospects of Alternative Transportation Fuels* (pp. 359-385). Springer, Singapore.

[2] Pickett, L.M. and Siebers, D.L., 2004. Non-sooting, low flame temperature mixing-controlled DI diesel combustion. SAE transactions, pp.614-630, DOI: 10.4271/2004-01-1399

[3] Lundgren, M., Wang, Z., Matamis, A., Andersson, O. et al., Effects of Post-Injections Strategies on UHC and CO at Gasoline PPC Conditions in a Heavy-Duty Optical Engine. SAE Technical Paper 2017-01-0753, 2017, DOI:10.4271/2017-01-0753.

[4] Song, X., Johnson, J. H., & Naber, J. D. (2015). A review of the literature of selective catalytic reduction catalysts integrated into diesel particulate filters. *International Journal of Engine Research*, *16*(6), 738-749, DOI: 10.1177/1468087414545094

[5] Nakatani K, Hirota S, Takeshima S, Itoh K, Tanaka T, & Dohmae K. Simultaneous PM and NOx reduction system for diesel engines. SAE technical paper 2002-01-0957, DOI: 10.4271/2002-01-0957

[6] Asanuma T, Hirota S, Yanaka M, Tsukasaki Y and Tanaka T. Effect of sulfur-free and aromatics-free diesel fuel on vehicle exhaust emissions using simultaneous PM and NOx reduction system. SAE technical paper 2003-01 1865, DOI: 10.4271/2003-01-1865

[7] Mizuno T and Suzuki J. Development of a new DPNR catalyst. SAE technical paper 2004-01-0578, DOI: 10.4271/2004-01-0578

[8] Kalghatgi, G., Risberg, P., and Ångström, H. Advantages of Fuels with High Resistance to Auto-ignition in Late-injection, Low-temperature, Compression Ignition Combustion. SAE Technical Paper, 2006-01-3385, DOI:10.4271/2006-01-3385

[9] Kim, K., Kim, D., Jung, Y., & Bae, C. (2013). Spray and combustion characteristics of gasoline and diesel in a direct injection compression ignition engine. *Fuel*, *109*, 616-626. DOI: 10.1016/j.fuel.2013.02.060

[10] G.T. Kalghatgi, P. Risberg, H.-E. Ångstr€om, Partially premixed auto-ignition of gasoline to attain low smoke and low NOx at high load in a compression ignition engine and comparison with a diesel fuel, SAE Technical Paper, 2007-01-0006, DOI: 10.4271/2007-01-0006

[11] López, J. J., García-Oliver, J. M., García, A., & Domenech, V. (2014). Gasoline effects on spray characteristics, mixing and auto-ignition processes in a CI engine under Partially Premixed Combustion conditions. *Applied Thermal Engineering*, *70*(1), 996-1006, DOI: 10.1016/j.applthermaleng.2014.06.027

[12] Solanki, V. S., Mustafi, N. N., & Agarwal, A. K. (2020). Prospects of Gasoline Compression Ignition (GCI) Engine Technology in Transport Sector. *Advanced Combustion Techniques and Engine Technologies for the Automotive Sector*, 77-110.

[13] Badra, J., Elwardany, A., Sim, J., Viollet, Y. et al. Effects of In-Cylinder Mixing on Low Octane Gasoline Compression Ignition Combustion. SAE Technical Paper 2016-01-0762, 2016, DOI: 10.4271/2016-01-0762.

[14] Jena, A., Singh, H., and Agarwal, A.K., 2021. Effect of Swirl Ratio and Piston Geometry on the Late-Compression Mean Air-Flow in a Diesel Engine. SAE Technical Paper, 2021-01-0647.

[15] Winroth, P.M. and Alfredsson, P.H., 2019. On shock structures in dynamic exhaust valve flows. Physics of Fluids, 31(2), p.026107, DOI: 10.1063/1.5084174

[16] Reddy, H. and Abraham, J., 2012. Two-dimensional direct numerical simulation evaluation of the flame-surface density model for flames developing from an ignition kernel in lean methane/air mixtures under engine conditions. Physics of Fluids, 24(10), p.105108, DOI: 10.1063/1.4757655

[17] Klein, M., Chakraborty, N., Jenkins, K.W. and Cant, R.S., 2006. Effects of initial radius on the propagation of premixed flame kernels in a turbulent environment. Physics of Fluids, 18(5), p.055102, DOI: 10.1063/1.2196092

[18] Kodavasal, J., Kolodziej, C. P., Ciatti, S. A., & Som, S. (2017). Effects of injection parameters, boost, and swirl ratio on gasoline compression ignition operation at idle

and low-load conditions. *International Journal of Engine Research*, *18*(8), 824-836, DOI: 10.1177/1468087416675709

[19] Dolak, J. G., Shi, Y., & Reitz, R. D. (2010). A computational investigation of stepped-bowl piston geometry for a light duty engine operating at low load. SAE Technical Paper, 2010-01-1263, DOI: 10.4271/2010-01-1263

[20] Fridriksson, H., Tuner, M., Andersson, O., Sunden, B. et al. Effect of Piston Bowl Shape and Swirl Ratio on Engine Heat Transfer in a Light-Duty Diesel Engine. SAE Technical Paper 2014-01-1141, 2014, DOI:10.4271/2014-01-1141.

[21] Pastor, J. V., García, A., Micó, C., Lewiski, F., Vassallo, A., & Pesce, F. C. (2021). Effect of a novel piston geometry on the combustion process of a light-duty compression ignition engine: An optical analysis. *Energy*, *221*, 119764, DOI: 10.1016/j.energy.2021.119764

[22] Cao, L., Bhave, A., Su, H., Mosbach, S., Kraft, M., Dris, A., & McDavid, R. M. (2009). Influence of injection timing and piston bowl geometry on PCCI combustion and emissions. *SAE International Journal of Engines*, *2*(1), 1019-1033, DOI: 10.4271/2009-01-1102

[23] Kook, S., Bae, C., Miles, P. C., Choi, D., Bergin, M., & Reitz, R. D. (2006). The effect of swirl ratio and fuel injection parameters on CO emission and fuel conversion efficiency for high-dilution, low-temperature combustion in an automotive diesel engine. *SAE Transactions*, 111-132, DOI: 10.4271/2006-01-0197

[24] Benajes, J., Martín, J., García, A., Villalta, D., & Warey, A. (2017). Swirl ratio and post injection strategies to improve late-cycle diffusion combustion in a light-duty diesel engine. *Applied Thermal Engineering*, *123*, 365-376 DOI: 10.1016/j.applthermaleng.2017.05.101

[25] Reitz, R. D., & Diwakar, R. (1987). Structure of high-pressure fuel sprays. *SAE transactions*, 492-509, DOI: 10.4271/870598

[26] Beale, J. C., & Reitz, R. D. (1999). Modeling spray atomization with the Kelvin-Helmholtz/Rayleigh-Taylor hybrid model. *Atomization and Sprays*, *9*(6), DOI: 10.1615/AtomizSpr.v9.i6.40

[27] Senecal, P. K., Pomraning, E., Richards, K. J., Briggs, T. E., Choi, C. Y., McDavid, R. M., & Patterson, M. A. (2003). Multi-dimensional modeling of direct-injection diesel spray liquid length and flame lift-off length using CFD and parallel detailed chemistry. *SAE transactions*, 1331-1351, DOI: 10.4271/2003-01-1043

[28] Liu, Y. D., Jia, M., Xie, M. Z., & Pang, B. (2012). Enhancement on a skeletal kinetic model for primary reference fuel oxidation by using a semi-decoupling methodology. *Energy & Fuels*, *26*(12), 7069-7083.

[29] N. Nordin, Numerical Simulations of Non-Steady Spray Combustion Using a Detailed Chemistry Approach. Thesis for the degree of Licentiate of Engineering, Dept. of Thermo and Fluid Dynamics, Chalmers University of Technology, Goteborg, Sweden, 1998

[30] Liu, Y. D., Jia, M., Xie, M. Z., & Pang, B. (2013). Development of a new skeletal chemical kinetic model of toluene reference fuel with application to gasoline surrogate fuels for computational fluid dynamics engine simulation. *Energy & fuels*, *27*(8), 4899-4909, DOI: 10.1021/ef4009955

[31] Kodavasal, J., Kolodziej, C., Ciatti, S., & Som, S. (2014, October). CFD simulation of gasoline compression ignition. In *Internal Combustion Engine Division Fall Technical Conference* (Vol. 46179, p. V002T06A008). American Society of Mechanical Engineers, DOI: 10.1115/ICEF2014-5591

[32] Najafabadi, M.I., Tanov, S., Wang, H., Somers, B., Johansson, B. and Dam, N., 2017. Effects of injection timing on fluid flow characteristics of partially premixed combustion based on high-speed particle image velocimetry. *SAE International Journal of Engines*, *10*(4), pp.1443-1453, DOI: 10.4271/2017-01-0744

[33] Agarwal, A.K., Gadekar, S. and Singh, A.P., 2017. In-cylinder air-flow characteristics of different intake port geometries using tomographic PIV. Physics of Fluids, 29(9), p.095104, DOI: 10.1063/1.5000725

[34] Dave, S., Anghan, C., Saincher, S., and Banerjee, J., 2021.Direct numerical simulation of forced turbulent round jet: Effect of flow confinement and varicose excitation, Physics of Fluids 33, 075108. doi: 10.1063/5.005435

[35] Sharma, N., Bachalo, W.D. and Agarwal, A.K., 2020. Spray droplet size distribution and droplet velocity measurements in a firing optical engine. Physics of Fluids, 32(2), p.023304. doi: 10.1063/1.5126498

[36] Tian, Y., Tian, Y., Shi, G., Zhou, B., Zhang, C. and He, L., 2020. Experimental study on oil droplet breakup under the action of turbulent field in modified concentric cylinder rotating device. Physics of Fluids, 32(8), p.087105.doi: 10.1063/5.0014002

[37] Mahmud, R., Kurisu, T., Nishida, K., Ogata, Y., Kanzaki, J., & Akgol, O. (2019). Effects of injection pressure and impingement distance on flat-wall impinging spray flame and its heat flux under diesel engine-like condition. *Advances in Mechanical Engineering*, *11*(7), 1687814019862910, DOI: 10.1177/1687814019862910

[38] Perini, F., Dempsey, A., Reitz, R.D., Sahoo, D., Petersen, B., and Miles, P.C., 2013. *A computational investigation of the effects of swirl ratio and injection pressure on mixture preparation and wall heat transfer in a light-duty diesel engine,* SAE Technical Paper 2013-01-1105, DOI: 10.4271/2013-01-1105

[39] Musculus, M.P., Miles, P.C. and Pickett, L.M., 2013. Conceptual models for partially premixed low-temperature diesel combustion. *Progress in energy and combustion science*, *39*(2-3), pp.246-283, DOI: 10.1016/j.pecs.2012.09.001

[40] Tang, Q., Liu, H., Li, M., Yao, M. and Li, Z., 2017. Study on ignition and flame development in gasoline partially premixed combustion using multiple optical diagnostics. *Combustion and Flame*, *177*, pp.98-108, DOI: 10.1016/j.combustflame.2016.12.013

[41] Raman, V., Tang, Q., An, Y., Shi, H., Sharma, P., Magnotti, G., Chang, J. and Johansson, B., 2020. Impact of spray-wall interaction on the in-cylinder spatial unburned hydrocarbon distribution of a gasoline partially premixed combustion engine. *Combustion and Flame*, *215*, pp.157-168, DOI: 10.1016/j.combustflame.2020.01.033

[42] Echekki, T. and Kolera-Gokula, H., 2007. A regime diagram for premixed flame kernel-vortex interactions. Physics of Fluids, 19(4), pp. 043604, DOI: 10.1063/1.3372167

[43] Dec, J.E., 1997. A conceptual model of DL diesel combustion based on laser-sheet imaging. *SAE transactions*, pp.1319-1348, DOI: 10.4271/970873

[44] Jawichian, A., Davoust, L., and Siedel., S., 2021. Dielectrophoresis-driven jet impingement heat transfers in microgravity conditions, Physics of Fluids 33, 073609 doi:10.1063/5.0055948

[45] Broatch, A., Novella, R., García-Tíscar, J., Gomez-Soriano, J. and Pal, P., 2020. Analysis of combustion acoustic phenomena in compression–ignition engines using large eddy simulation. Physics of Fluids, 32(8), p.085101.doi: 10.1063/5.0011929

## Abbreviation

| | |
|---|---|
| LTC | Low-temperature Combustion |
| PCI | Premixed Compression Ignition |
| GCI | Gasoline compression ignition |
| CI | Compression ignition |
| CDC | Conventional diesel combustion |
| HCCI | Homogeneous charge compression ignition |
| RCCI | Reactivity controlled compression ignition |
| PCCI | Premixed charge compression ignition |
| RoPR | Rate of pressure rise |
| SR | Swirl ratio |
| PRR | Pressure rise rate |
| AHR | Apparent heat release |
| HRR | Heat release rate |
| TKE | Turbulent kinetic energy |
| SoC | Start of combustion |
| aTDC | After top dead center |
| bTDC | Before top dead center |
| LTHR | Low-temperature heat release |
| HTHR | High-temperature heat release |

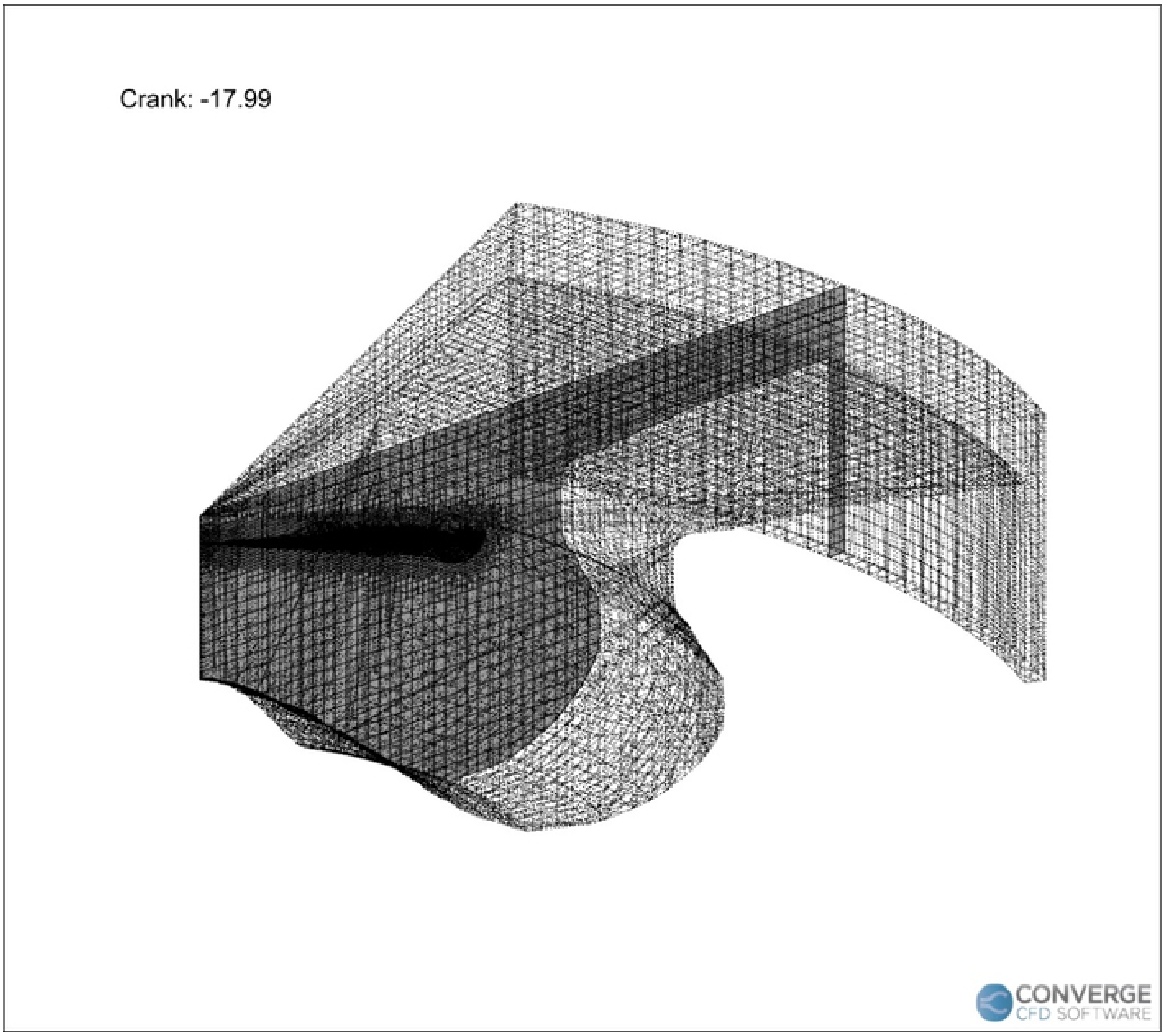
Crank: -17.99
CONVERGE
CFD SOFTWARE

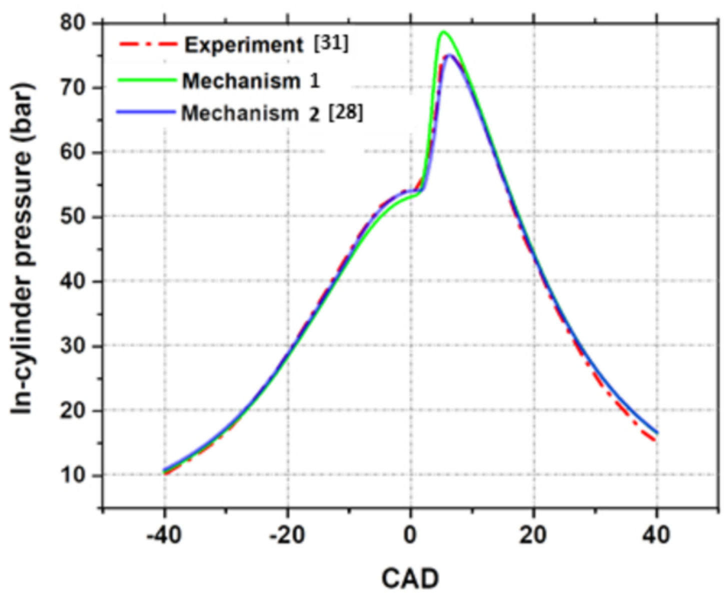
Experiment [31]
Mechanism 1
Mechanism 2 [28]
In-cylinder pressure (bar)
CAD
80
70
60
50
40
30
20
10
-40
-20
0
20
40

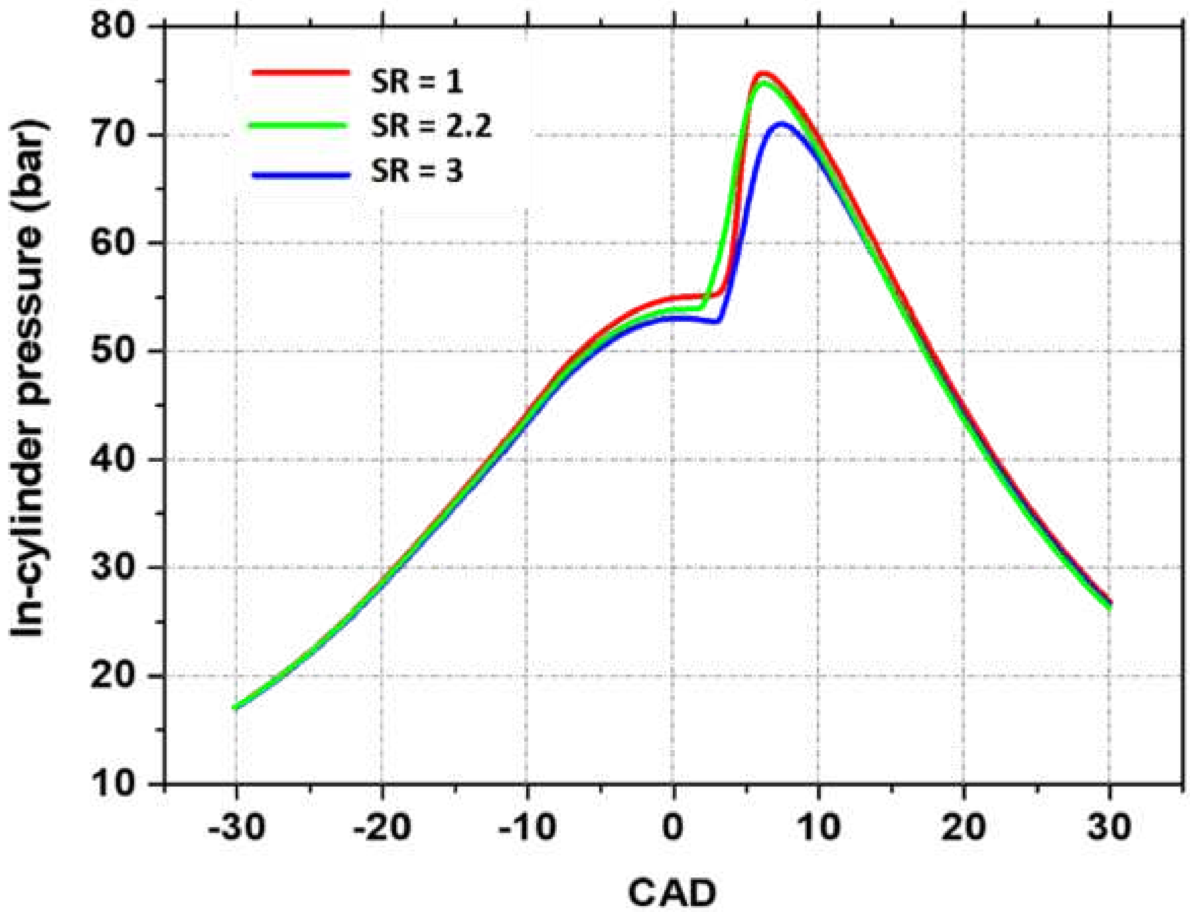
SR = 1
SR = 2.2
SR = 3
In-cylinder pressure (bar)
CAD
80
70
60
50
40
30
20
10
-30
-20
-10
0
10
20
30

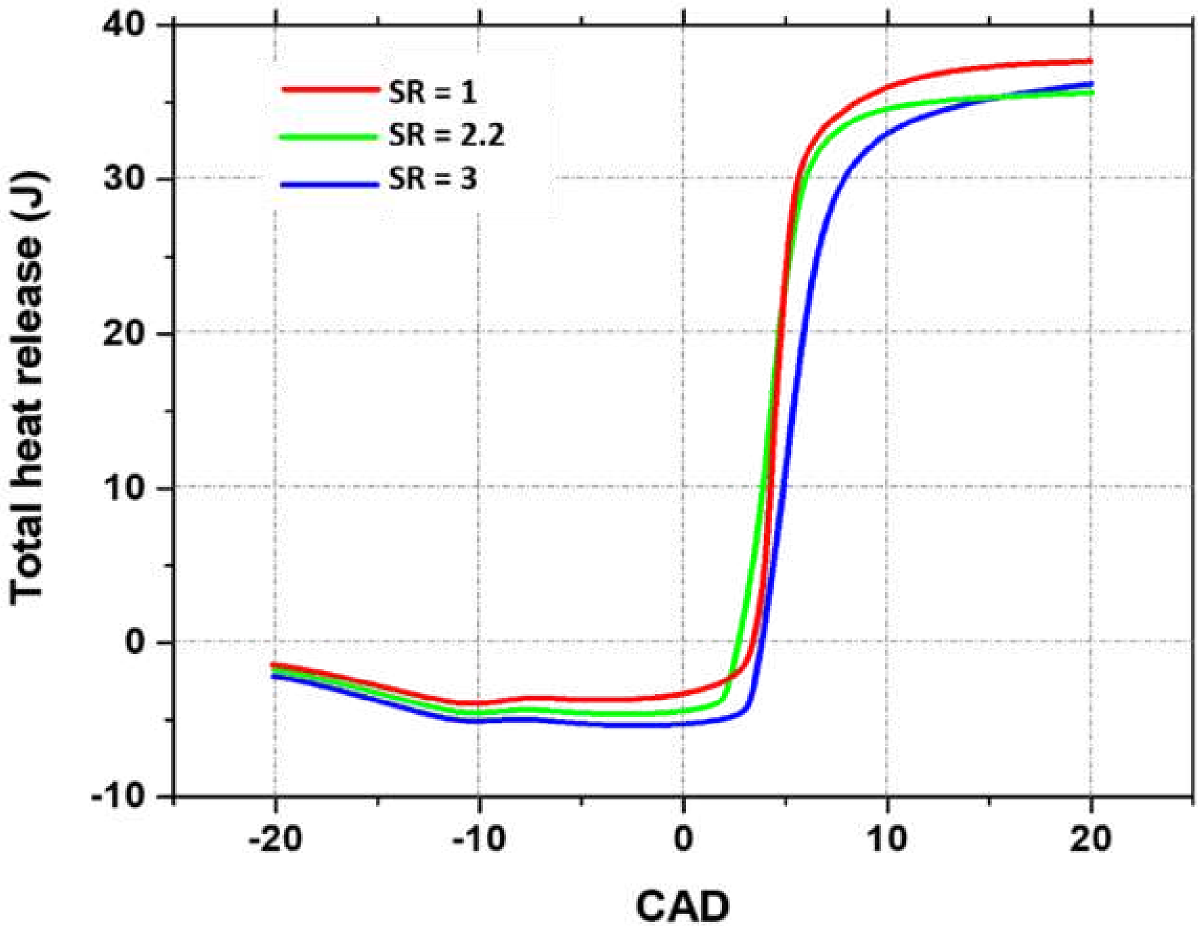
SR = 1
SR = 2.2
SR = 3
Total heat release (J)
CAD
40
30
20
10
0
-10
-20
-10
0
10
20

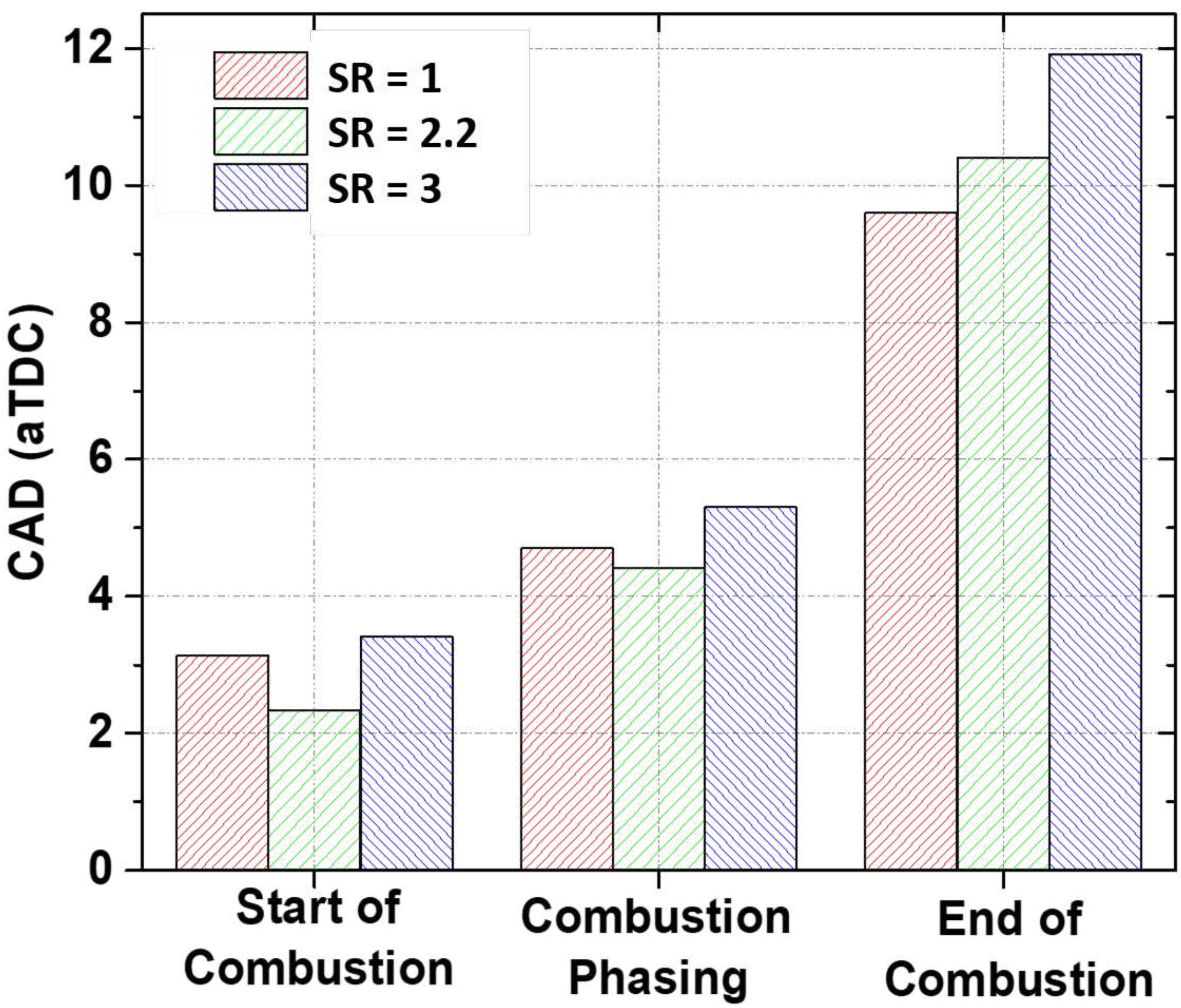
SR = 1
SR = 2.2
SR = 3
CAD (aTDC)
0
2
4
6
8
10
12
Start of Combustion
Combustion Phasing
End of Combustion

PLEASE CITE THIS ARTICLE AS DOI: 10.1063/5.0059579

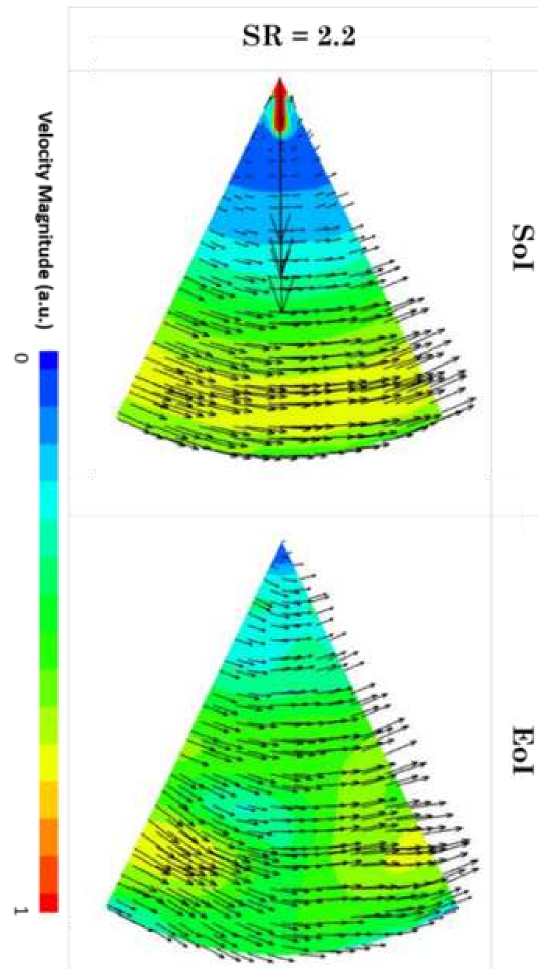

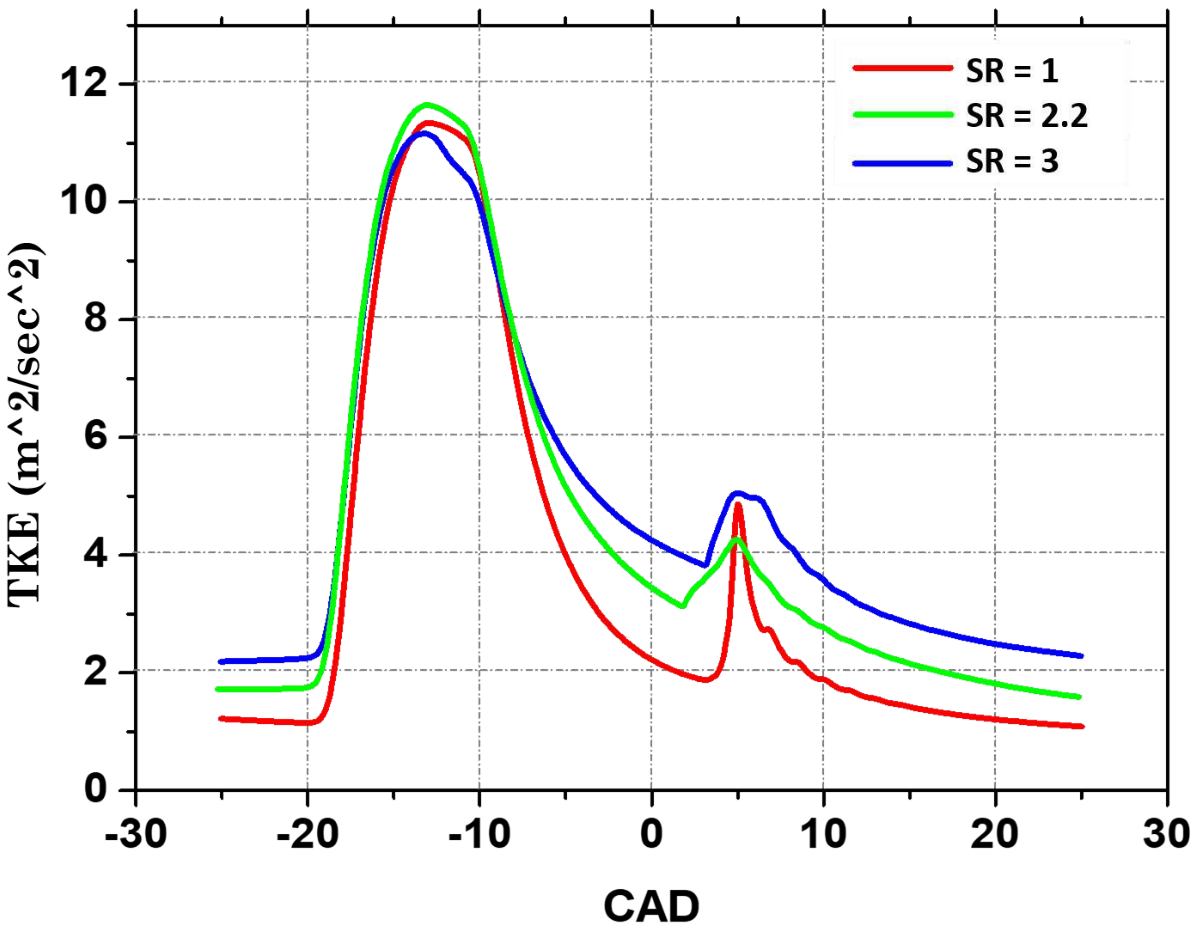
SR = 1
SR = 2.2
SR = 3
TKE (m^2/sec^2)
CAD
0
2
4
6
8
10
12
-30
-20
-10
0
10
20
30

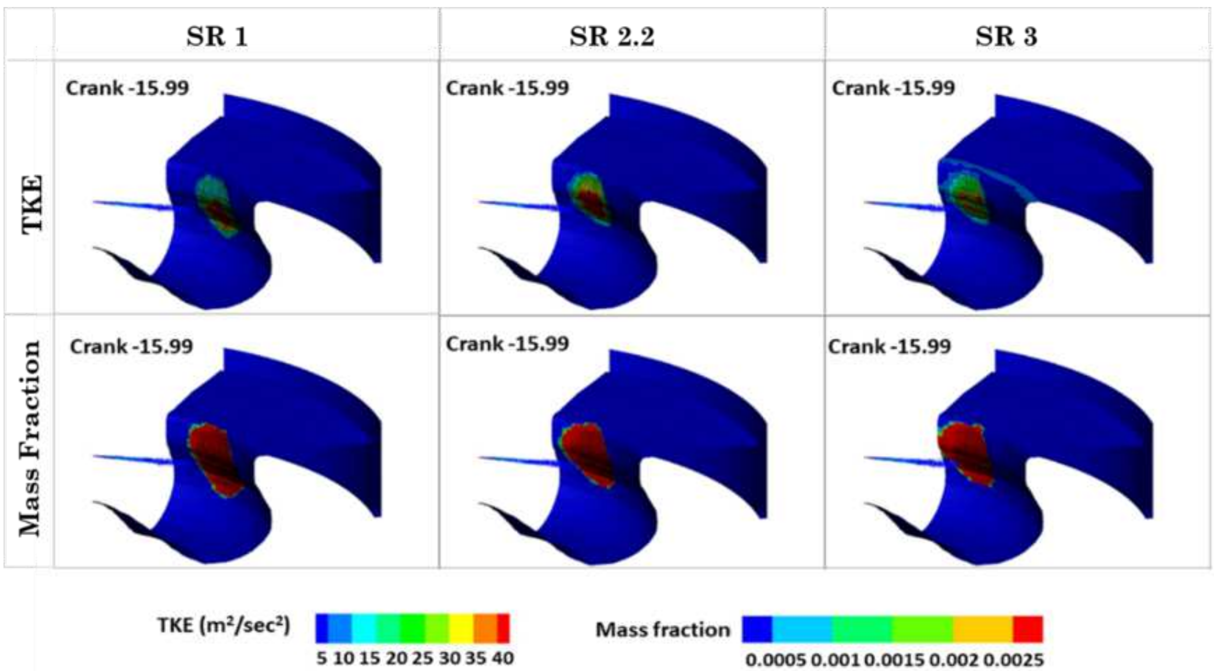
SR 1
SR 2.2
SR 3
TKE
Mass Fraction
Crank -15.99
Crank -15.99
Crank -15.99
Crank -15.99
Crank -15.99
Crank -15.99
TKE (m²/sec²)
5 10 15 20 25 30 35 40
Mass fraction
0.0005 0.001 0.0015 0.002 0.0025

PLEASE CITE THIS ARTICLE AS DOI: 10.1063/5.0059579

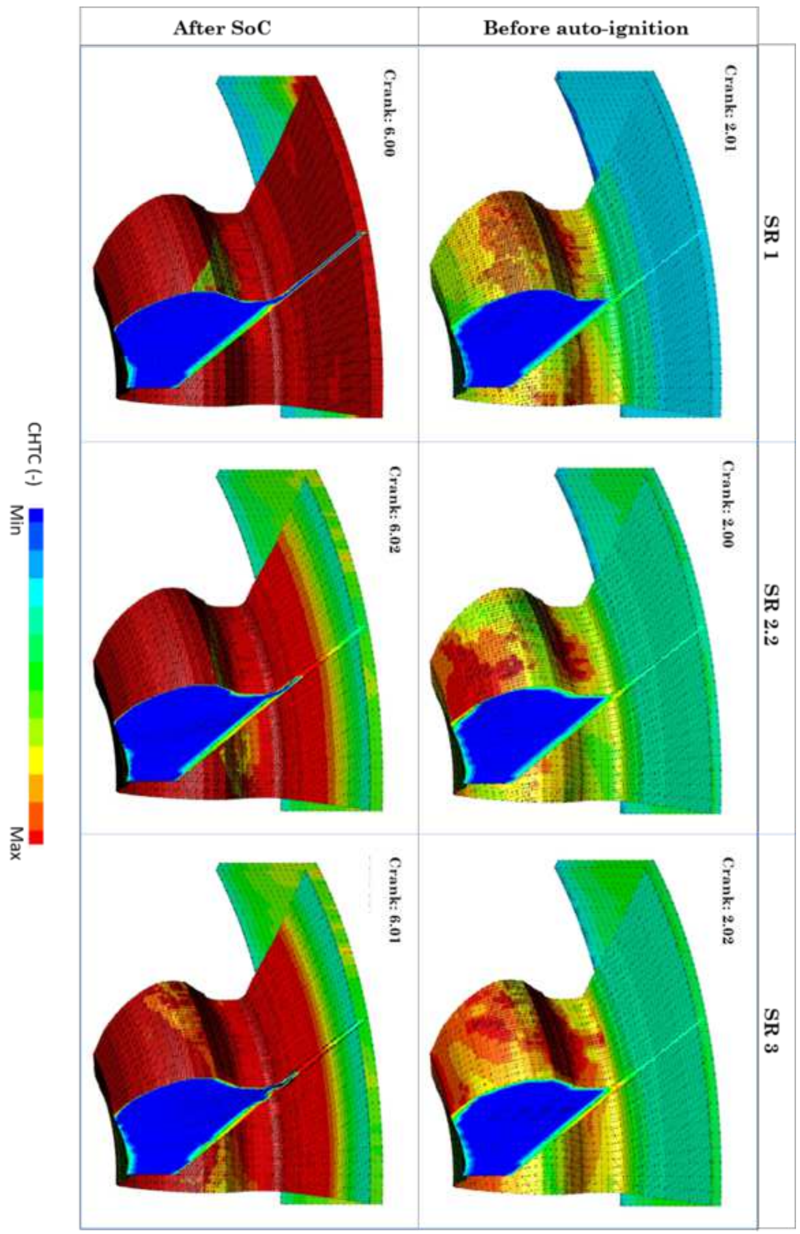

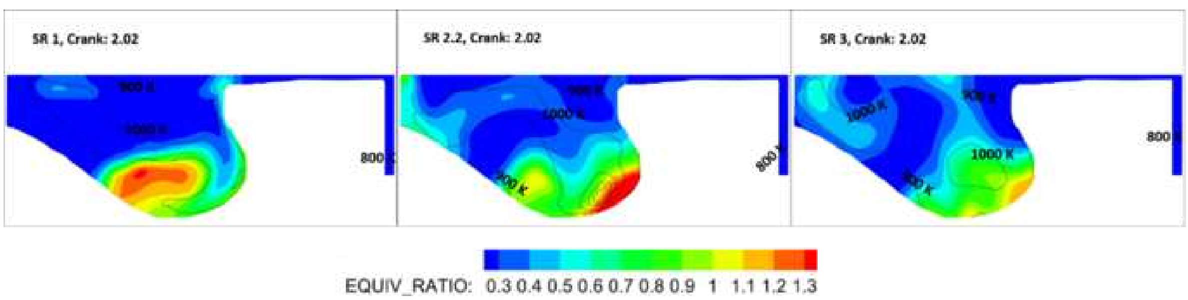
SR 1, Crank: 2.02
SR 2.2, Crank: 2.02
SR 3, Crank: 2.02
900 K
1000 K
800 K
EQUIV_RATIO: 0.3 0.4 0.5 0.6 0.7 0.8 0.9 1 1.1 1.2 1.3

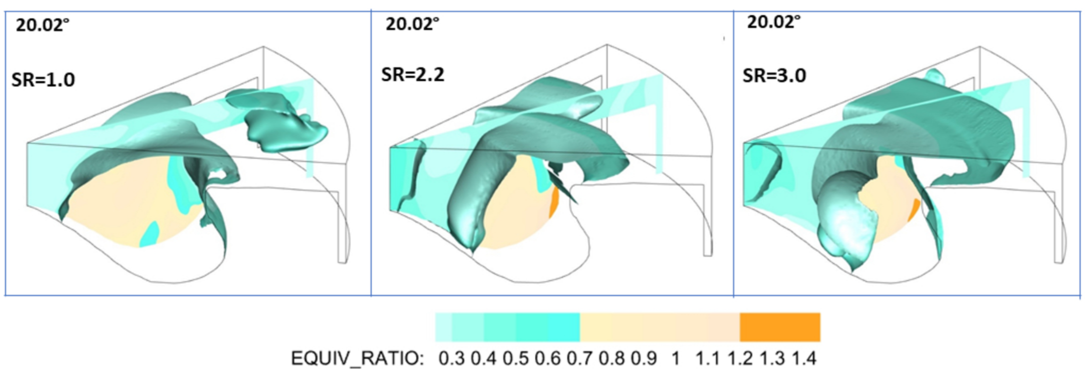
20.02°
SR=1.0
20.02°
SR=2.2
20.02°
SR=3.0
EQUIV_RATIO: 0.3 0.4 0.5 0.6 0.7 0.8 0.9 1 1.1 1.2 1.3 1.4

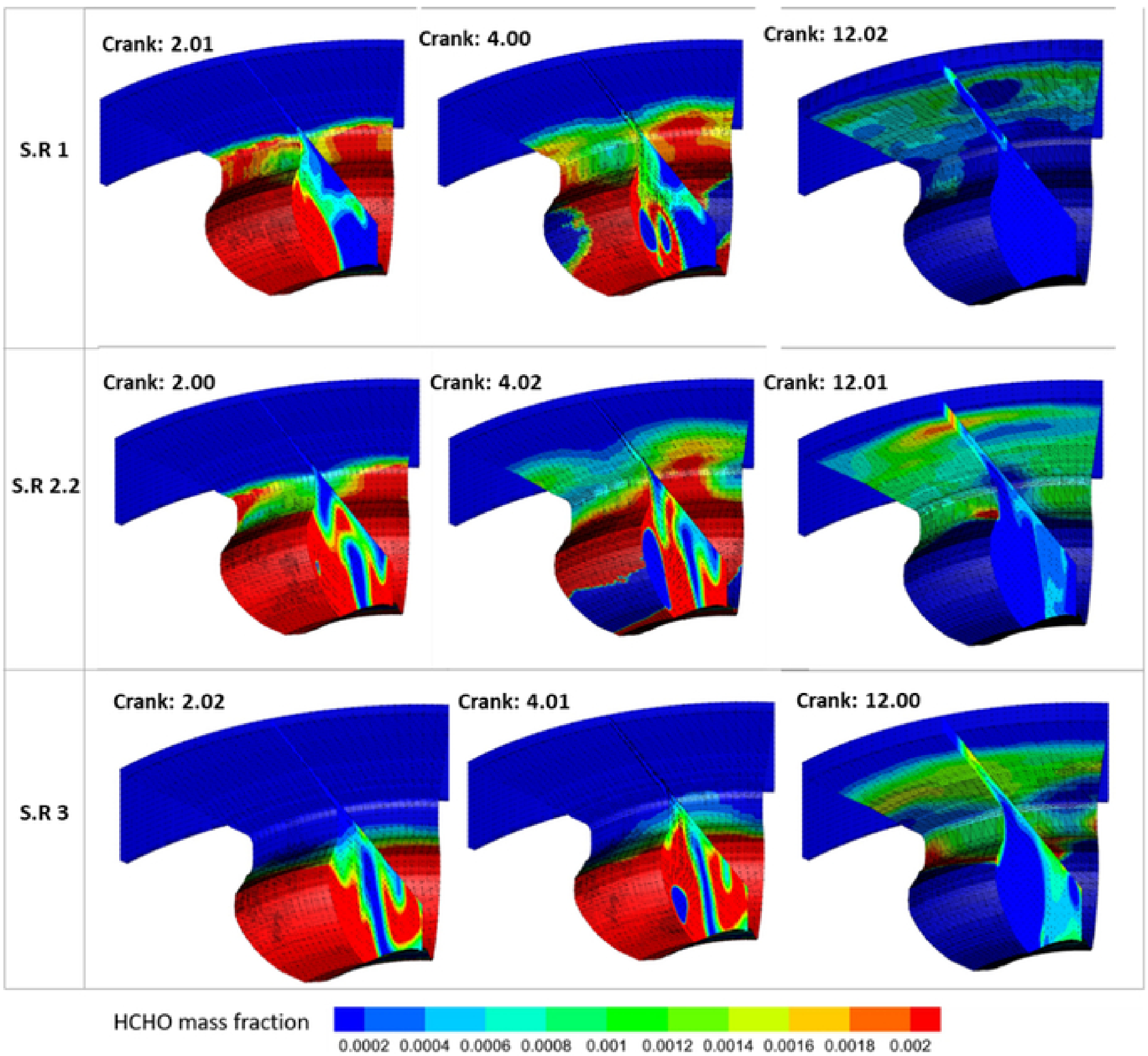
Crank: 2.01
Crank: 4.00
Crank: 12.02
S.R 1
Crank: 2.00
Crank: 4.02
Crank: 12.01
S.R 2.2
Crank: 2.02
Crank: 4.01
Crank: 12.00
S.R 3
HCHO mass fraction
0.0002 0.0004 0.0006 0.0008 0.001 0.0012 0.0014 0.0016 0.0018 0.002

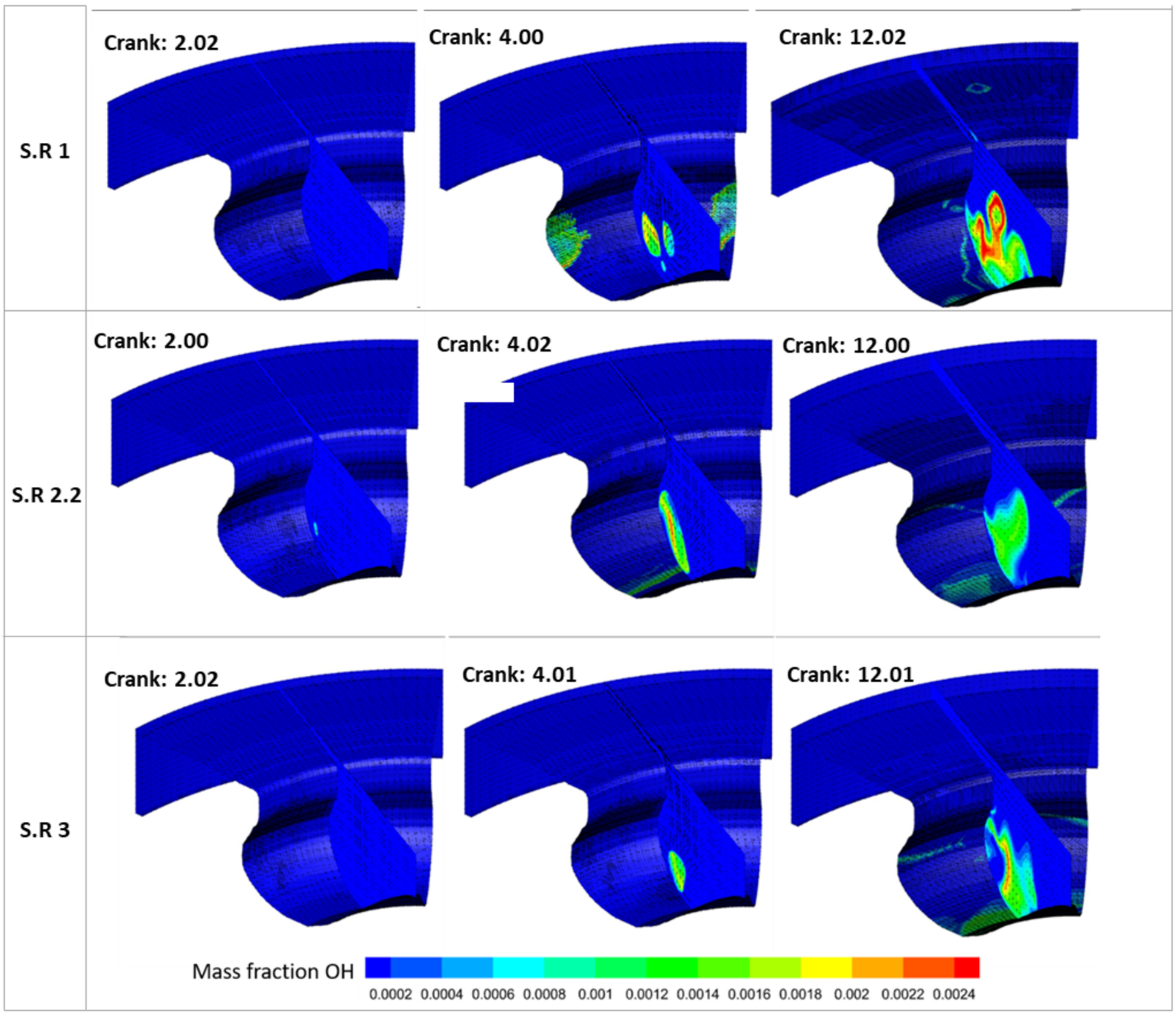
S.R 1
Crank: 2.02
Crank: 4.00
Crank: 12.02
S.R 2.2
Crank: 2.00
Crank: 4.02
Crank: 12.00
S.R 3
Crank: 2.02
Crank: 4.01
Crank: 12.01
Mass fraction OH
0.0002 0.0004 0.0006 0.0008 0.001 0.0012 0.0014 0.0016 0.0018 0.002 0.0022 0.0024